

# What can we learn from the surface chemical composition of the optical companions of Soft X-ray transients?

Ene Ergma<sup>1,2</sup> and Marek J. Sarna<sup>3</sup>

<sup>1</sup> Physics Department, Tartu University, Ülikooli 18, 50090 Tartu, Estonia

<sup>2</sup> Astronomical Observatory, Helsinki University, Box 14, 00014 Helsinki, Finland  
email: ene@physic.ut.ee

<sup>3</sup> N. Copernicus Astronomical Center, Polish Academy of Sciences, ul. Bartycka 18, 00-716 Warsaw, Poland.  
email: sarna@camk.edu.pl

Received ;accepted

**Abstract.** Several evolutionary sequences with low-mass secondaries ( $M_d=1.25, 1.5$  and  $1.7 M_\odot$ ) and black hole accretors ( $M_{bh}=5$  and  $10 M_\odot$ ) are calculated. The angular momentum losses due to magnetic braking and gravitational wave radiation are included. Using full nuclear networks (p-p and CNO cycles) we follow carefully the evolution of the surface composition of the secondary star. We find that the surface chemical composition of the secondary star may give additional information which helps to understand the formation of soft X-ray transients with black holes as accretors. We show that observations of isotope ratios  $^{12}\text{C}/^{13}\text{C}$ ,  $^{14}\text{N}/^{15}\text{N}$  and  $^{16}\text{O}/^{17}\text{O}$  with comparison to computed sequences allow estimates independent from spectroscopy of the mass of the secondary component. We find that our evolutionary calculations satisfactorily explain the observed  $q = M_{sg}/M_{bh} - P_{orb}$  distribution for Soft X-ray transients with orbital periods less than one day. Using our evolutionary calculations we estimate secondary masses and surface chemical abundances (C,N,O) for different systems. We distinguished three different phases in the SXT's evolution. The optical component shows (i) cosmic C, N, O abundances and  $^{12}\text{C}/^{13}\text{C}$  isotopic ratio; (ii) cosmic C, N, O abundances but modified  $^{12}\text{C}/^{13}\text{C}$  ratio; and (iii) depletion of C and enhanced of N abundances and strongly modified isotopic ratios of C, N, O elements.

**Key words.** stars: evolution – chemical evolution – soft X-ray transients – black holes

## 1. Introduction

In recent years, about a dozen of black hole candidates (BHC) with low-mass companion stars have been identified as the so-called soft X-ray transients (SXTs). During the low X-ray luminosity stage (quiescent phase) optical/infrared observations of the optical companion allow the measurement of the mass function and sets a strong lower limit to the mass of the unseen companion

$$f(M_{bh}) = \frac{M_{bh}^3 \sin^3 i}{(M_{bh} + M_{sg})^2} = \frac{K_{sg}^3 P_{orb}}{2\pi G} \quad (1)$$

where  $M_{bh}$ ,  $M_{sg}$  are the black hole and secondary masses,  $i$  is the inclination of the binary orbit,  $P_{orb}$  is the orbital period and  $K_{sg}$  is the velocity semi-amplitude of the optical component.

If  $f(M_{bh}) > 3 M_\odot$ , then  $M_{bh}$  is larger than the upper limit to the gravitational mass of a neutron star (Rhoades

& Ruffini 1974) and these compact objects are black holes. The total number of close binaries with a black hole companion in the Galaxy is estimated to be between a few hundred and a few thousand. Only a small fraction of these systems shows X-ray activity (Tanaka & Lewin 1995, Tanaka & Shibazaki 1996).

The most popular scenario for the origin of low-mass X-ray binaries proposes as starting point a relatively wide binary system with extreme mass ratio (van den Heuvel 1983). After filling its Roche lobe, the massive primary engulfs its low-mass companion which will spiral-in inside its envelope (common envelope). In the common envelope scenario, if the envelope of the massive star is expelled before the low-mass secondary coalesces with the massive helium core of the primary then a close binary system forms. Black hole formation occurs due to the collapse of massive helium core after the ejection of the red supergiant envelope.

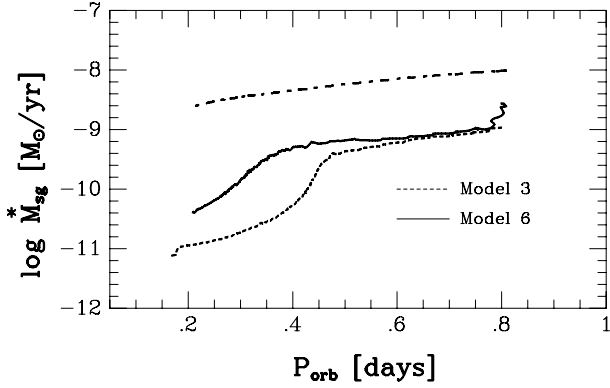


**Fig. 1.** The evolution of mass accretion rate as a function of the orbital period: dashed line – model 3, solid line – model 6. The critical mass accretion rate computed from Eq. (2) is also shown (dash-dotted line).

The critical question is which stars end their evolution with black hole formation.

For a long time it has been accepted that black holes form from very massive stars (more than  $40\text{--}50M_{\odot}$ ). Recently observational and theoretical evidence suggest that black holes form from stars with masses above  $25M_{\odot}$  (Portegies Zwart, Verbunt & Ergma 1997, Ergma & van den Heuvel 1998, Ergma & Fedorova 1998, Fryer 1999).

The majority of observed black hole candidates (see Table 1) have orbital periods less than one day. Therefore, the transient nature of BHC systems and short orbital periods put rather strong constraints on the properties of the progenitor systems and hence our understanding on how these systems evolve.

In this paper we would like to show that there is one additional, independent observational piece of evidence – the abundance of CNO elements and their isotopic ratios – which will give us information about the progenitors of SXTs and their evolutionary stage.

## 2. LMXB evolution – general picture

Following the King, Kolb & Burderi (1996) description we discuss three cases of evolution depending on two timescales: 1) nuclear expansion of the secondary on the timescale  $\tau_{ms}$  and 2) shrinkage of the orbit on the angular momentum loss timescale  $\tau_{aml}$ . In Case (1)  $\tau_{ms} \ll \tau_{aml}$ , in Case (2)  $\tau_{ms} \gg \tau_{aml}$ , and in Case (3)  $\tau_{ms} \sim \tau_{aml}$ . For Case (1) the secondary evolves as a subgiant (or giant) and transfers mass on the nuclear timescale. The binary is evolving to longer periods and after mass transfer ceases a wide system with a black hole and a helium white dwarf is formed. A similar evolutionary scenario has been discussed for the formation of wide binary millisecond pulsars with helium white dwarfs (see recent results by Tauris & Savonije 1999). As shown by King et al. (1996) for Case (2) the secondary is an unevolved main-sequence star and the mass transfer rate is always above the limit mass transfer rate (Equation (2)) for an irradiated disk, i.e. the mass transfer is stable. The binary evolves to short peri-

ods (hours) and is observed as a persistent X-ray source. In Case (3), the secondary is evolved before mass transfer starts, but angular momentum losses shrink the binary orbit more rapidly than it expands and the binary evolves to very short periods (Ergma & Fedorova 1998).

To understand why these sources are transients we use the dwarf nova instability criterion adapted to account for X-ray heating of the disk. King, Kolb & Szuszkiewicz (1997) have realized that heating by irradiation is much weaker if the accreting object is a black hole rather than a neutron star, since the black hole has no hard surface and cannot act as a point source for irradiation. For black hole binaries King et al. (1997) have obtained the following formula for the critical accretion rate

$$\dot{M}_{cr}^{irr} \approx 2.86 \times 10^{-11} M_{bh}^{5/6} M_{sg}^{-1/6} P_{orb}^{4/3} [M_{\odot} yr^{-1}] \quad (2)$$

For  $\dot{M} < \dot{M}_{cr}^{irr}$  mass transfer is unstable and the source will show transient outbursts. So we may exclude Case (2) in our consideration since for this case the mass transfer rate is stable and the binary is observed as a persistent but not a transient X-ray source.

Ergma & Fedorova (1998) found the bifurcation period  $P_{bif}$ , which separates orbital evolution of Case (3) and Case (2) from Case (1) to be about one day. So to have short orbital period systems it is necessary that the secondary fills its Roche lobe (RLOF) with initial orbital period  $P_{i,orb}(RLOF)$  less than  $P_{bif}$ . Also, the mass of secondary is not arbitrary but must be between 1 and  $1.8M_{\odot}$  to have Case (2) or (3) evolution. Pylyser & Savonije’s (1988) calculations show an absence of Case (2) or (3) evolution for a binary consisting of  $M_{bh} = 4M_{\odot}$  with initial donor star mass  $\geq 1.7M_{\odot}$ .

## 3. The evolutionary code

The Roche-filling-component (secondary star) models were computed using a standard stellar evolution code based on the Henyey-type code of Paczyński (1970), which has been adapted to low-mass stars (Marks & Sarna 1998). The carbon-nitrogen-oxygen (CNO) tri-cycle affects the abundance ratios we are interested in outside the hydrogen burning core. As the secondary loses matter, due to mass transfer, layers originally below the surface are exposed. As a consequence of mass loss and nuclear evolution, a convective envelope develops and penetrates to even deeper layers of the star, which are then mixed, changing its surface chemical composition.

Our nuclear reaction network is based on that of Kudryashov & Ergma (1980), who included the reactions of the CNO tri-cycle in their calculations of hydrogen and helium burning in the envelope of an accreting neutron star. We have included the reactions of the proton-proton (p-p) chain. Hence we are able to follow the evolution of the elements  $^1\text{H}$ ,  $^3\text{He}$ ,  $^4\text{He}$ ,  $^7\text{Be}$ ,  $^{12}\text{C}$ ,  $^{13}\text{C}$ ,  $^{13}\text{N}$ ,  $^{14}\text{N}$ ,  $^{15}\text{N}$ ,  $^{14}\text{O}$ ,  $^{15}\text{O}$ ,  $^{16}\text{O}$ ,  $^{17}\text{O}$  and  $^{17}\text{F}$ . We assume that the abundances of  $^{18}\text{O}$  and  $^{20}\text{Ne}$  stay constant throughout the evolution. We use the reaction rates of

**Table 1.** Observational data for SXT with known orbital periods ( $< 1$  d)

Sources	$P_{orb}$ [d]	q	$f(M_{bh})$ [ $M_{\odot}$ ]	i	References
XTE J1118+480	0.171		$6.0 \pm 0.3$		McClintock et al. 2000, 2001
		$\sim 0.05$	$6.1 \pm 0.3$	$81 \pm 2$	Wagner et al. 2001
GRO J0422+32	0.212	$0.116^{+0.079}_{-0.071}$	$1.21 \pm 0.06$	35–55	Harlaftis et al. 1999
			$1.19 \pm 0.02$		Webb et al. 2000
GRS 1009–45	0.285	$0.137 \pm 0.015$	$3.17 \pm 0.12$	$< 80$	Filippenko et al. 1999
A0620–00	0.323	$0.067 \pm 0.010$	$3.18 \pm 0.16$	31–54	Marsh et al. 1994
GS 2000+25	0.345	$0.042 \pm 0.012$	$4.97 \pm 0.10$	66	Casares et al. 1995, Harlaftis et al. 1996
GRS 1124–683	0.433	$0.128^{+0.044}_{-0.039}$	$3.10 \pm 0.4$	54–65	Casares et al. 1997
H1705–250	0.521	$< 0.053$	$4.86 \pm 0.13$	60–80	Harlaftis et al. 1997
4U 1755–338	0.186	BHC			Pan et al. 1995
XTE J1859+226	0.382	BHC			Sanchez-Fernandez et al. 2000
GX339–4	0.617	BHC			Tanaka & Lewin 1995

Fowler, Caughlan & Zimmerman (1967, 1975), Harris et al. (1983), Caughlan et al. (1985), Caughlan & Fowler (1988), Bahcall & Ulrich (1988), Bahcall & Pinsonneault (1992), Bahcall, Pinsonneault & Wasserburg (1995) and Pols et al. (1995).

For radiative transport, we use the opacity tables of Iglesias & Rogers (1996). Where the Iglesias & Rogers (1996) tables are incomplete, we have filled the gaps using the opacity tables of Huebner et al. (1977). For temperatures less than 6000 K we use the opacities given by Alexander & Ferguson (1994) and Alexander (private communication). The contribution from conduction, which is present in the Huebner et al. (1977) opacity tables, has been added to the other tables as well, since they don't include it (Haensel, private communication). The chemical compositions  $X=0.7$ ,  $Z=0.02$ . In calculating evolutionary models of binary stars, we must take into account mass transfer and the associated physical mechanisms which lead to angular momentum loss. We consider the subsequent mass transfer from the secondary to the black hole when the secondary star reaches contact with its Roche lobe. We use the Eggleton (1983) formula to calculate the size of the secondary's Roche lobe. We take into account angular momentum losses due to gravitational wave radiation (Landau & Lifshitz 1971) and magnetic stellar wind braking (Verbunt & Zwaan 1981).

#### 4. Observational data

In Table 1 we present observational data for all known or suspected SXTs with a black hole as accretor and orbital period less than one day.

Spectral observations and a mass function determination have been done for several systems. For a few systems C, N, O spectral lines in different wavelength ranges were also detected.

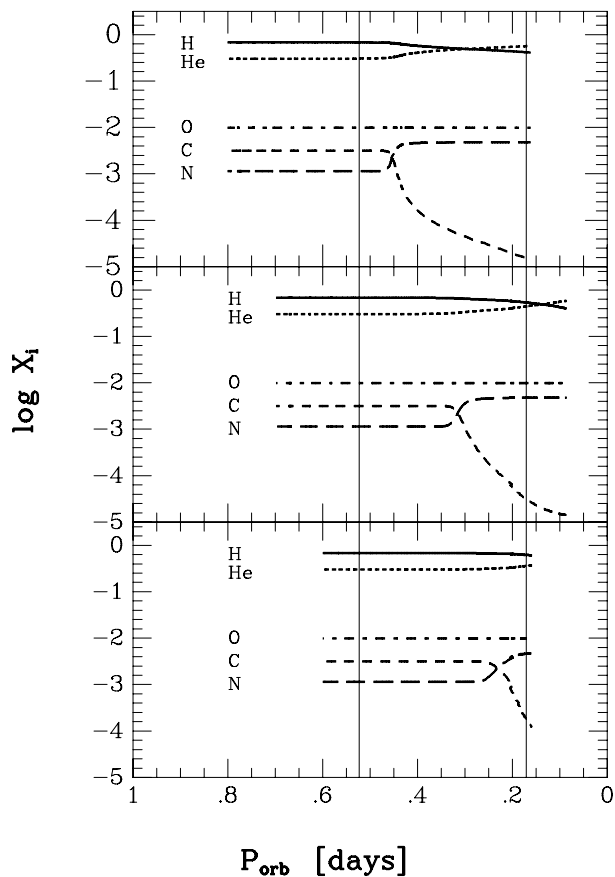


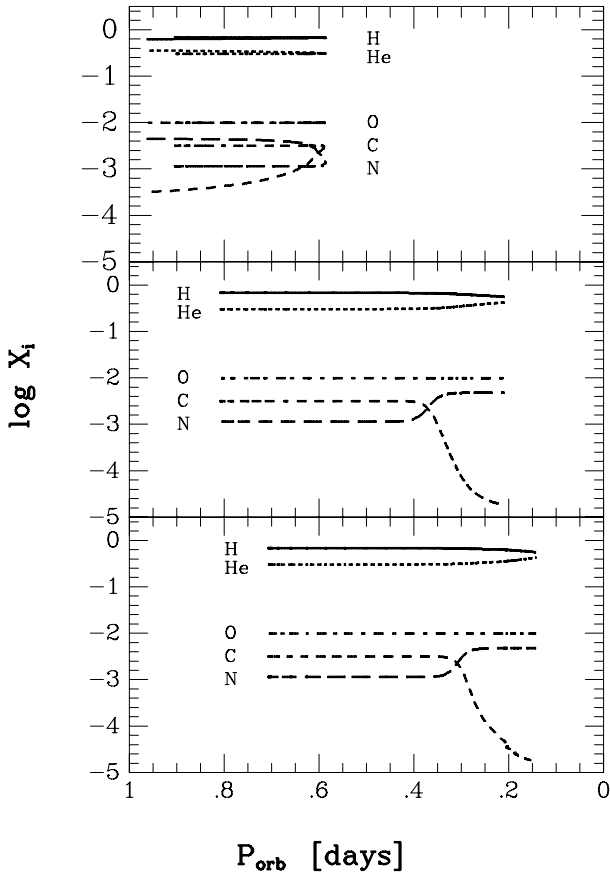
**Fig. 2.** The evolution of the red subgiant surface abundances of H, He, O, C, N as a function of orbital period: lower panel – sequence (1), middle panel – sequence (2), upper panel – sequence (3). The two thin solid vertical lines show the orbital period region for SXT's.

##### 4.1. XTE J1118+480

XTE J1118+480 is BHC (Table 1) with an orbital period of 0.171 d (Patterson 2000). McClintock et al. (2000, 2001) found that  $f(M_{bh})=6.0 \pm 0.36 M_{\odot}$ . Similar result has been

**Table 2.** The computed sequences

Model	$P_{i,orb}$ (RLOF) [d]	$P_{orb}$ (C/N=1) [d]	$P_{orb}$ (C/N=0.1) [d]	$M_{i,bh}$ [ $M_{\odot}$ ]	$M_{i,sg}$ [ $M_{\odot}$ ]	$M_{sg}$ (C/N=1) [ $M_{\odot}$ ]	$M_{sg}$ (C/N=0.1) [ $M_{\odot}$ ]
1	0.6	0.234	0.191	10	1.25	0.472	0.346
2	0.7	0.315	0.277	10	1.25	0.488	0.365
3	0.8	0.455	0.431	10	1.25	0.514	0.353
4	0.7	0.295	0.249	5	1.25	0.487	0.372
5	0.7	0.277	0.309	10	1.50	0.624	0.505
6	0.8	0.373	0.336	10	1.50	0.636	0.505
7	0.9	0.791	0.599	10	1.50	0.671	0.599
8	0.8	0.347	0.312	5	1.50	0.632	0.507
9	0.8	0.442	0.394	10	1.70	0.749	0.610
10	0.8	0.410	0.355	5	1.70	0.746	0.611

**Fig. 3.** The same as for Fig. 2: lower panel – sequences (5), middle panel – sequences (6), upper panel – sequence (7)

presented by Wagner et al. (2001) ( $f(M_{bh}) = 6.1 \pm 0.3 M_{\odot}$ ). Haswell, Hynes & King (2000) found that the Balmer jump appears in absorption. N V emission (124.0, 124.3 nm) is most prominent with equivalent width 0.6 nm. No C IV or O V emission is detected, suggesting that the accreting material has been CNO-processed.

#### 4.2. XTE J1859+226

XTE J1859+226 is suspected BHC with suggested orbital period  $P_{orb} = 0.382$  d (Sanchez-Fernander et al. 2000). The ultraviolet spectrum shows broad and deep Ly- $\alpha$  absorption, strong C IV 155.5 nm emission and weaker emission lines of C III, N V, O III, O IV, O V, Si IV and He II (Hynes et al. 1999).

#### 4.3. 4U 1755–338

The spectrum is nearly featureless. Very weak He II was measured in one spectrum in 1986 (Cowley, Hutchings & Crampton 1988).

#### 4.4. GRS 1124–68

Della Valle, Jarvis & West (1991) found that the most prominent emission lines are  $H_{\alpha}$ ,  $H_{\beta}$ , N III+He II and N II (721.7 nm). The N III emission is normally attributed to the X-ray heating driving the Bowen fluorescence process, but in the present case it appears broadened by the O II and C III ions.

### 5. Results of calculations

In Table 2 we present computed masses and orbital periods for two different phases of the binary evolutionary sequences: for the beginning of carbon depletion (C/N=1) and the high carbon depletion (C/N=0.1).

In our Table 2 only for Model 7 the secondary fills Roche lobe close to the bifurcation period and binary evolution ends up with almost the same period as the initial orbital period. For other models, since  $P_{i,orb}(RLOF) < P_{bif}$  all binaries evolve towards short orbital periods. In Fig. 1 we present mass accretion rate versus orbital period for Models 3 and 6. The critical mass accretion rate (Equation (2)) is also shown (dash-dotted line). Our calculations show that during evolution the secular mass accretion rate is always less than the critical one. Ergma & Fedorova (1998) pointed out that the

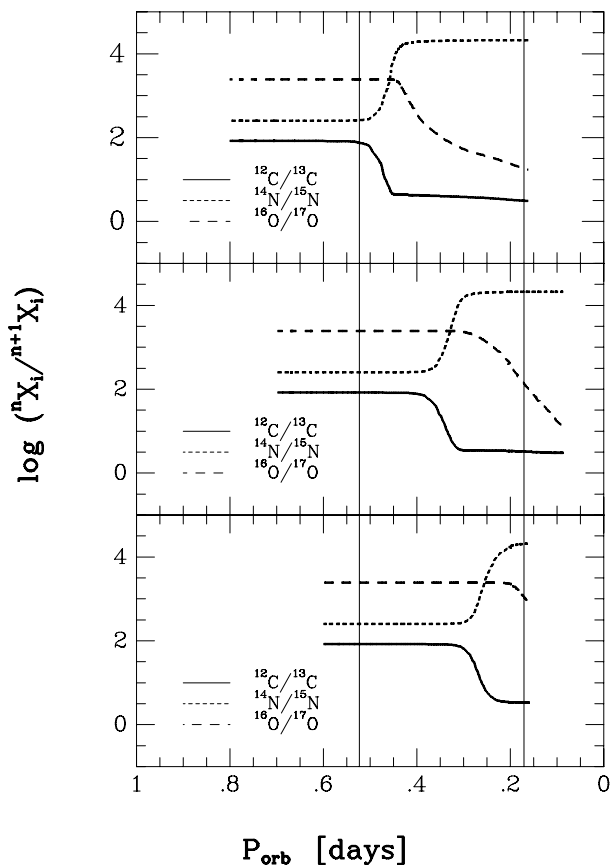


**Fig. 4.** The evolution of various isotope ratios  $^{12}\text{C}/^{13}\text{C}$ ,  $^{14}\text{N}/^{15}\text{N}$  and  $^{16}\text{O}/^{17}\text{O}$  versus orbital period for  $1.25 M_{\odot}$  secondary: lower panel – sequence (1), middle panel – sequence (2), upper panel – sequence (3). The two thin solid vertical lines show the orbital period region for SXT’s.

condition for disk instability is more favorable in systems with higher black hole masses.

Our main interest was concerned with how the surface chemical composition evolves depending on the initial secondary mass and the initial orbital period of RLOF. In Fig. 2a, b, c we present the evolution of the  $1.25 M_{\odot}$  red subgiant surface abundances of H, He, O, C, N as a function of orbital period for Models 1, 2 and 3. In Fig 3a, b, c the same is shown but for  $1.5 M_{\odot}$  secondaries (Models 5, 6, 7).

Figures 2 and 3 show that surface chemical composition may give us additional information about the progenitors of SXTs. If we do not observe carbon in the spectra of the optical companion of SXTs with orbital period about 0.4 d, then the secondary must fill its Roche lobe near  $P_{i,orb}(RLOF) \geq 0.8$  d (but less than one day). The secondary initial mass must be less than  $1.7 M_{\odot}$ . We predict that if we observe carbon in the spectra of the secondary star in SXT with  $P_{orb} \simeq 0.3$  d, then the initial mass of the secondary must be less than  $1.5 M_{\odot}$  (Fig.3). For  $M_{sg} = 1.25 M_{\odot}$ , initial Roche lobe filling must occur when  $P_{i,orb}(RLOF) \leq 0.6$  d. In Figs. 4a, b, c and 5a, b, c the dependence of various isotope ratios  $^{12}\text{C}/^{13}\text{C}$ ,  $^{14}\text{N}/^{15}\text{N}$  and  $^{16}\text{O}/^{17}\text{O}$  versus orbital period are shown.

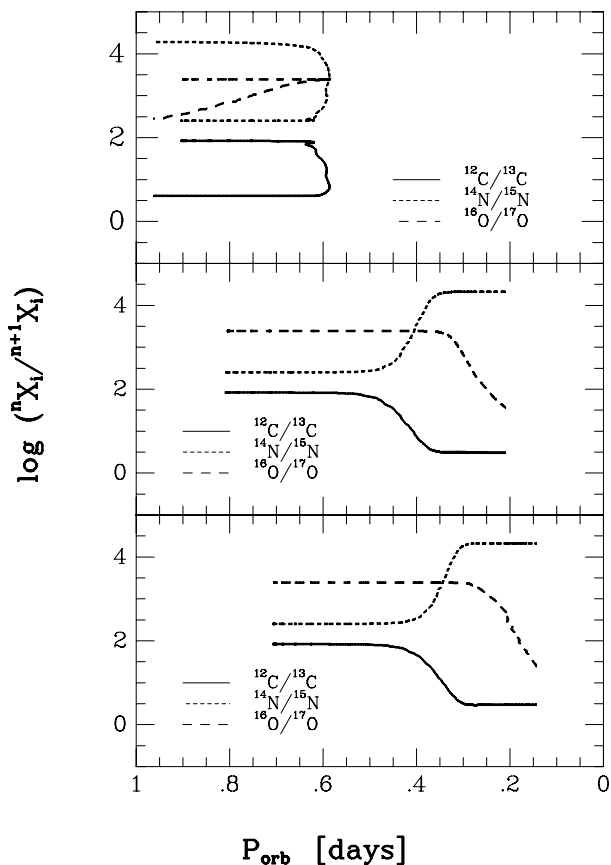


**Fig. 5.** The same as for Fig. 4 but for  $1.5 M_{\odot}$  secondary: lower panel – sequence (5), middle panel – sequence (6), upper panel – sequence (7)

In Fig. 6a, b we show the evolution of the red subgiant surface abundances of H, He, O, C, N (a) and  $^{12}\text{C}/^{13}\text{C}$ ,  $^{14}\text{N}/^{15}\text{N}$  and  $^{16}\text{O}/^{17}\text{O}$  (b) as a function of secondary mass (Model 3). In Fig. 7a, b the same is shown for Model 6. From these figures we can see that for more massive secondaries isotope ratios start to change when the mass of the secondary has decreased to  $0.9 M_{\odot}$  ( $0.7 M_{\odot}$  for a less massive secondary) and C/N ratios change when  $M_{sg} \leq 0.6 M_{\odot}$  (for  $1.5 M_{\odot}$ ) and  $M_{sg} \leq 0.5 M_{\odot}$  (for  $1.25 M_{\odot}$ ) independent of the initial period of the RLOF.

From the point of view of the chemical composition evolution we will distinguish three different phases of the SXT’s evolutionary stage:

- 1) For  $M_{sg} > 0.7 M_{\odot}$  and  $P_{orb} > 0.4$  d the optical component shows solar/cosmic C, N, O abundances and isotopic ratio of  $^{12}\text{C}/^{13}\text{C}$ .
- 2) For  $0.4 M_{\odot} < M_{sg} < 0.7 M_{\odot}$  and  $0.3$  d  $< P_{orb} < 0.4$  d the optical component shows cosmic C, N, O abundances but modified  $^{12}\text{C}/^{13}\text{C}$  ratio.
- 3) For  $M_{sg} < 0.4 M_{\odot}$  and  $P_{orb} < 0.3$  d the optical component shows depletion of carbon and enhanced of N abundances (small C/N ratio) and strongly modified isotopic ratios of C, N, O elements.

We conclude that chemical evolution can give us extra information on the mass of the secondary and this is inde-

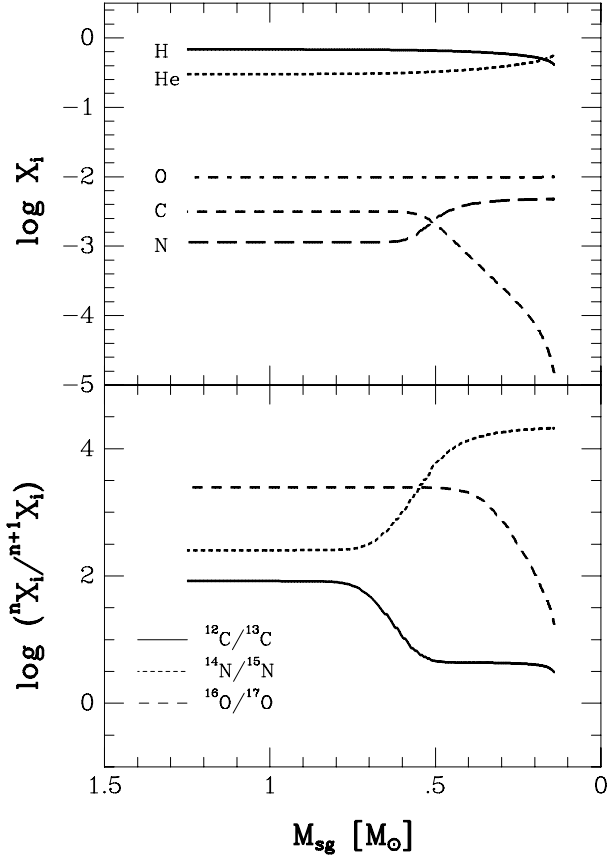


**Fig. 6.** The evolution of red subgiant surface abundances of H, He, O, C (upper panel) and isotopic ratios of  ${}^{12}\text{C}/{}^{13}\text{C}$ ,  ${}^{14}\text{N}/{}^{15}\text{N}$  and  ${}^{16}\text{O}/{}^{17}\text{O}$  (lower panel) as function of secondary mass (Model 3).

pendent of the black hole mass and the initial evolutionary stage of the secondary component (see Table 2).

### 5.1. Comparison with observations

In Fig. 8 we present calculated  $q$  versus orbital period  $P_{orb}$  for  $M_{sg}=1.70, 1.50, 1.25 M_{\odot}$  and  $M_{bh}=5M_{\odot}$  (upper curves) and  $M_{bh}=10 M_{\odot}$  (lower curves). In this figure we also plot observed  $q$  values from Table 1. We see that for five systems (XTE J1118+480, A0620-003, GS 2000+25, GRS 1124-683 and H1705-250 (only upper limit)) our theoretical results agree satisfactorily with the observations. For GRO J0422+32 and GRS 1009-45 agreement is not good. The mass ratio for GRS 1009-45 is based only on an  $H_{\alpha}$  emission radial velocity curve that is not exactly in antiphase with respect to the absorption line velocity curve. Therefore this mass ratio should be treated with extreme caution (referee remark). The mass ratio for GRS 1009-45 is not reliable so that point in  $q - P_{orb}$  diagram can move down (good for theoretical models) or up (bad for our picture). For XTE J1118+480 Wagner et al. (2001) found that modeling of the light curves gives a small mass ratio ( $\sim 0.05$ ) which fits well with our model calculation results (see also Fig.8).

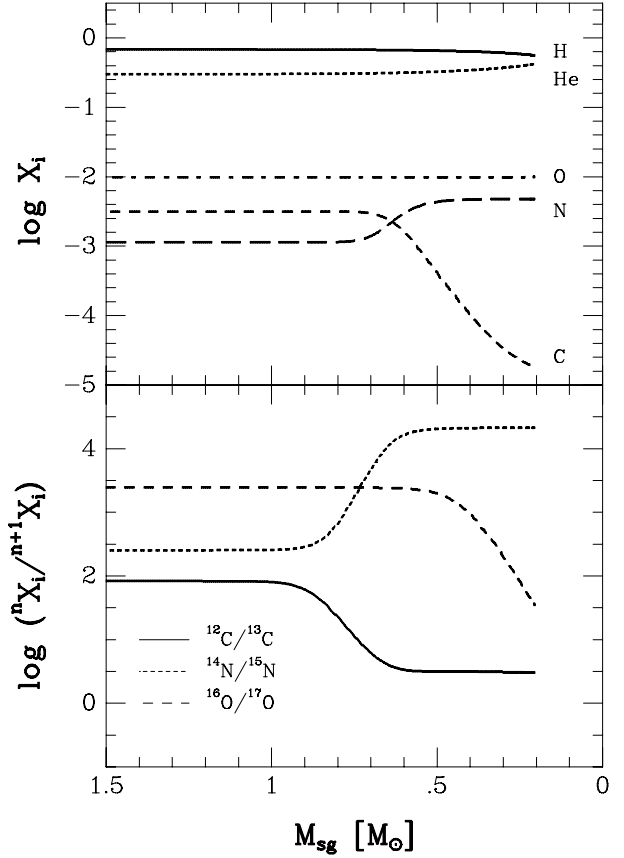


**Fig. 7.** The same as for Fig. 7 but for model 6.

In Fig. 9 computed mass functions (for different values of orbital inclination) are shown for two black hole masses (5 and  $10M_{\odot}$ ) and three secondary masses (1.25, 1.5 and  $1.7M_{\odot}$ ).

From computed evolutionary sequences we predict the chemical composition of the optical companion of the black hole. For all systems with known orbital period (see Table 1) we estimate (from our grid of models) the following parameters: C/N,  ${}^{12}\text{C}/{}^{13}\text{C}$ ,  ${}^{16}\text{O}/{}^{17}\text{O}$  and  $M_{sg}$ . The data are presented in Table 3. For all systems we predict the range of secondary masses using only orbital period and our grid of models.

All our models (beside Model 7) predict that near orbital period 0.2-0.3 d carbon is depleted (GRO J0422+32 and XTE J1118+480). For XTE J1118+480 we estimate a secondary mass in the range  $0.14-0.29 M_{\odot}$  and a rather small mass ratio ( $q < 0.04$ ).

If XTE J1859-058 has an orbital period of 0.382 d and its UV spectrum shows carbon emission lines then besides the Models 3,7,9 and 10 carbon is not depleted near this orbital period.

### 5.2. Observational tests

Besides the UV and blue spectral regions it is interesting to try to observe in red spectral regions (Charles 2001, private communication) and infrared regions of the spectrum.

**Table 3.** The predicted chemical composition and secondary masses of SXTs with orbital periods  $< 1$  d

Sources	$P_{orb}$ [d]	C/N	$^{12}\text{C}/^{13}\text{C}$	$^{16}\text{O}/^{17}\text{O}$	$M_{sg}$ [ $M_{\odot}$ ]
XTE J1118+480	0.171	0.005–0.04	3–3.4	20–1100	0.14–0.29
GRO J0422+32	0.212	0.004–0.02	3–3.4	30–500	0.15–0.36
GRS 1009–45	0.285	0.01–1.14	3.1–3.8	50–2000	0.17–0.54
A0620–00	0.323	0.005–1.6	3–5.2	70–2470	0.18–0.67
GS 2000+25	0.345	0.02–2.78	10–83	100–2470	0.20–0.83
GRS 1124–683	0.433	0.12–2.78	4–83	1600–2470	0.36–1.05
H1705–250	0.521	2.78	74–83	2470	0.77–1.24
4U 1755–338	0.186	0.005–0.09	3–3.4	20–1800	0.15–0.33
XTE J1859+226	0.382	0.03–2.78	7–83	200–2470	0.25–0.90
GX339–4	0.617	2.78	83	2470	0.94–1.25

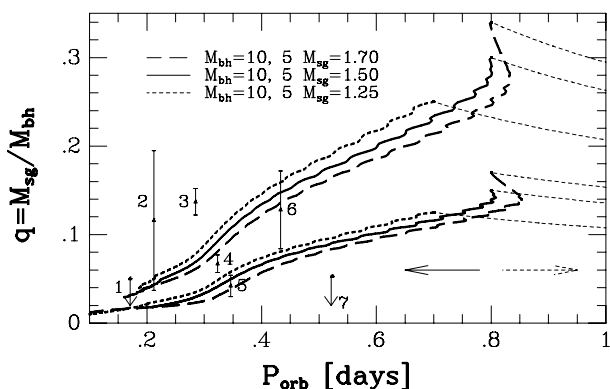


**Fig. 8.** The observed mass ratio  $q$  versus orbital period  $P_{orb}$  for black hole X-ray transients: 1 – XTE J1118+480, 2 – GRO J0422+32, 3 – GRS 1009–45, 4 – A0620–003, 5 – GS 2000+25, 6 – GRS 1124–683, 7 – H1705–250. The calculated theoretical relations  $(q, P_{orb})$  for various  $M_{bh}$  and  $M_{sg}$  are also plotted. Thin dashed lines show fully conservative evolution. The two arrows show the directions of non-conservative (solid) and fully conservative (dashed) evolution. Upper curves are for  $M_{bh} = 5 M_{\odot}$ , lower for  $M_{bh} = 10 M_{\odot}$ .

### 5.2.1. Red observations of the CN bands

The red CN bands  $A^2\Pi - X^2\Sigma^+$  (Bauschlicher, Langhoff & Taylor 1988) from 4370–15050Å is useful for observations. We propose to observe spectral region near 7920–7940Å to identify two  $^{13}\text{CN}$  lines at 7921.13Å and 7935.67Å which are very useful for both  $^{12}\text{C}/^{13}\text{C}$  isotopic ratio and C, N abundances determination. It revealed that in the case of low  $^{12}\text{C}/^{13}\text{C}$  ratio ( $< 10$ ) these lines is clearly recognized (Fujita 1985). However, in stars of high  $^{12}\text{C}/^{13}\text{C}$  ratio ( $> 20$ ) both isotopic lines is undetectable. The best candidates for such observations are GRS 1009–45, A0620–00 and GRS 1124–683. The  $E_{B-V}$  in the direction of these systems is not very high and also optical companions are not too faint. For first two systems we predict no carbon detection while for last one carbon lines must be visible.

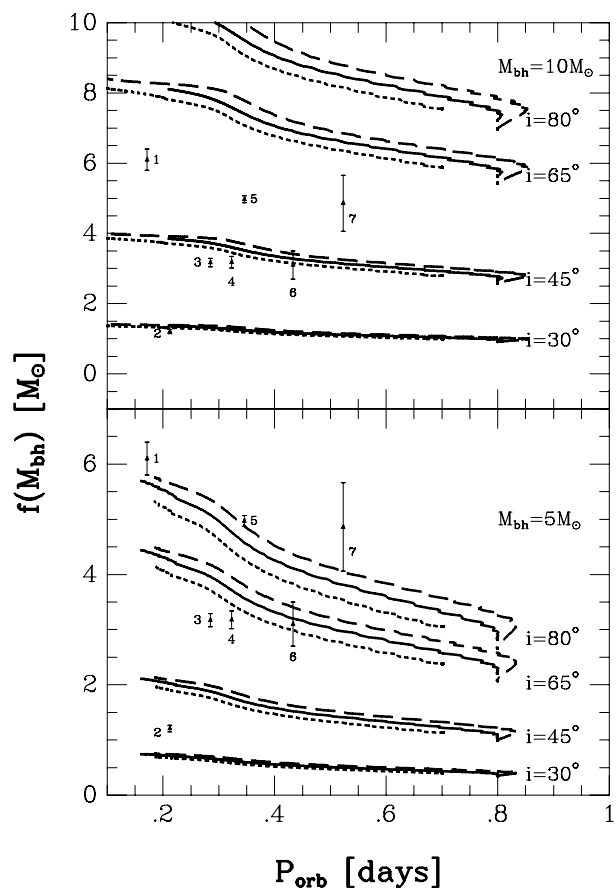


**Fig. 9.** The observed mass function  $f(M_{bh})$  versus orbital period  $P_{orb}$  for black hole X-ray transients: 1 – XTE J1118+480, 2 – GRO J0422+32, 3 – GRS 1009–45, 4 – A0620–003, 5 – GS 2000+25, 6 – GRS 1124–683, 7 – H1705–250. The calculated theoretical relations  $(f(M_{bh}), P_{orb})$  are for  $M_{bh} = 10 M_{\odot}$  and  $M_{sg} = 1.25$  (short-dashed lines), 1.5 (solid lines) and  $1.7 M_{\odot}$  (long-dashed lines) (upper panel).  $i = 30, 45, 65, 80$  are also marked. The same for  $M_{bh} = 5 M_{\odot}$  and  $M_{sg} = 1.25$  (short-dashed lines), 1.5 (solid lines) and  $1.7 M_{\odot}$  (long-dashed lines) (lower panel).

### 5.2.2. Infrared observations of the CO bands

Following Sarna et al. (1995), Marks, Sarna & Prialnik (1997) and Marks & Sarna (1998) the isotopic ratios  $^{12}\text{C}/^{13}\text{C}$  and  $^{16}\text{O}/^{17}\text{O}$  can be determined by infrared observations of the CO bands. Specifically, the bands of  $^{12}\text{CO}$  and  $^{13}\text{CO}$  around 1.59, 2.3 (2.29, 2.32, 2.35 and 2.38  $\mu\text{m}$ ) and 4.6  $\mu\text{m}$  (Bernat et al. 1979, Harris & Lambert 1984a, b, Harris, Lambert & Smith 1988) give a direct measurement of the isotopic ratio  $^{12}\text{C}/^{13}\text{C}$ . If we can estimate also the  $^{16}\text{O}/^{17}\text{O}$  ratio then it is possible to determine the secondary mass using computed sequences. For such observations 10m class telescope is necessary.

## 6. Conclusions

Our theoretical models show that observations of chemical abundances may give additional information about the progenitors of SXTs and also about the mass of the secondary component. To produce the majority observed short orbital period SXTs with a black hole as accretor, the initial secondary mass must be between 1 and 1.7  $M_{\odot}$  and the initial orbital period (when the secondary is filling its Roche lobe) between 0.5 and 1 d. It will be interesting to do population synthesis analyses to see how many systems it is possible to produce in the suggested orbital period – secondary mass range. Having data about observed C, N, O and their isotopes abundances it is possible to estimate the mass of the secondary component. Non-conservative evolution (in a sense of the orbital angular momentum loss from the system) is able to explain satisfactorily the observed mass ratio and orbital period distributions. From our analysis one can conclude that the black hole masses are between 5 and 10  $M_{\odot}$  which agrees well with Bailyn et al. (1998) results who compiled the observations of the mass functions and the best estimates of the mass ratios and inclinations and concluded that the black hole masses were clustered near 7  $M_{\odot}$ .

### ACKNOWLEDGEMENTS

EE thanks Dr. D.Hannikainen for careful reading this paper and useful remarks. EE acknowledges warm hospitality of the Astronomical Observatory Helsinki University where this paper was prepared. MJS thanks prof. P. Charles for very useful discussions during his stay in University of Southampton. We thank anonymous referee for his/hers very constructive referee opinion which really improve the text of this paper. This work was partially supported by a grant N 157992 from the Academy of Finland to Dr. Osmi Vilhu and ESF grant N 4338. At Warsaw, this work has been supported through grants 2-P03D-014-13 and 2-P03D-005-16 by the Polish National Committee for Scientific Research and by the NATO Collaborative Linkage Grant PST.CLG.977383.

### References

Alexander D. R. & Ferguson J. W., 1994, ApJ, 437, 879

- Alexander D. R., 1995, private communication  
 Bahcall J. N. & Pinsonneault M. H., 1992, Rev. Mod. Phys., 64, 885  
 Bahcall J. N. & Ulrich R. K., 1988, Rev. Mod. Phys., 60, 297  
 Bahcall J. N. Pinsonneault M. H. & Wasserburg G. J., 1995, Rev. Mod. Phys., 67, 781  
 Bailyn Ch. D. Jain R. K. Coppi P. & Orosz J. A., 1998, ApJ., 499,367  
 Bauschlicher C. W. Langhoff S. R. & Taylor P. R., 1988, ApJ, 332, 531  
 Bernat A. P. Hall D. N. B. Hinkle K. H. & Ridgway S. T., 1979, ApJ, 233, L135  
 Casares J. Charles P. A. & Marsh T. R., 1995, MNRAS, 277, L45  
 Casares J. Martin E. L. Charles P. A. Molaro P. & Rebolo R., 1997, New Astronomy 1,299  
 Caughlan G. R. Fowler W. A. Harris M. J. & Zimmerman B. A., 1985, Atom. Data and Nucl. Data Tables, 32, 197  
 Caughlan G. R. & Fowler W. A., 1988, Atom. Data and Nucl. Data Tables, 40, 283  
 Cowley A. P. Hutchings J. B. & Crampton D., 1988, ApJ, 333, 906  
 Della Valle M. Jarvis B. & West R., 1991, Nat., 353, 50  
 Eggleton P.P., 1983, ApJ, 268, 368  
 Ergma E. & van den Heuvel E. P. J., 1998, A&A, 331, L29  
 Ergma E. & Fedorova A., 1998, A&A, 338, 69  
 Filippenko A. V. Leonard D. C. Matheson T. Li W. Moran E. C. & Riess A. G., 1999, PASP, 111, 969  
 Fowler W. A. Caughlan G. R. & Zimmerman B. A., 1967, ARA&A, 5, 525  
 Fowler W. A. Caughlan G. R. & Zimmerman B. A., 1975, ARA&A, 13, 69  
 Fryer C. L., 1999, ApJ, 522, 413  
 Fujita Y., 1985, in: “Cool Stars with Excesses of Heavy Elements”, eds. M. Jaschek and P. C. Keenan, Dordrecht, Reidel, p. 31  
 Harlaftis E. T. Horne K. & Filippenko A. V., 1996, PASP, 108, 762  
 Harlaftis E. T. Steeghs I. Horne K. & Filippenko A. V., 1997, AJ, 114, 1170  
 Harlaftis E. Collier S. Horne K. & Filippenko A. V., 1999, A&A, 341, 491  
 Harris M. J. & Lambert D. L., 1984a, ApJ, 281,739  
 Harris M. J. & Lambert D. L., 1984b, ApJ, 285,674  
 Harris M. J. Fowler W. A. Caughlan G. R. & Zimmerman B. A, 1983, ARA&A, 21, 165  
 Harris M. J. Lambert D. L. & Smith V. V., 1988, ApJ, 325, 768  
 Haswell C. A., Hynes R. I. & King A. R., 2000, IAUC no. 7407  
 Huebner W. F. Merts A. L. Magee N. H. Jr. & Argo M. F., 1977, Astrophys. Opacity Library, Los Alamos Scientific Lab. Report No. LA-6760-M  
 Hynes R. I. Haswell C. A. Norton A. J. & Chaty S., 1999, IAUC no. 7279  
 Iglesias C. A. & Rogers F. J., 1996, ApJ, 464, 943  
 King A. R. Kolb U. & Burderi L., 1996, ApJ, 464, L127  
 King A. R. Kolb U. & Szuszkiewicz E., 1997, ApJ, 488,89  
 Kudryashov A. D. & Ergma E. V., 1980, Sov. Astron. Lett., 6, 375  
 Landau L. D. & Lifshitz E. M., 1971, “Classical theory of fields”. Pergamon Press, Oxford  
 Maeder A., 1992, A&A, 264, 105  
 Marks P. B., Sarna M. J. & Prialnik D., 1997, MNRAS, 290, 283



- Marks P. B. & Sarna M. J., 1998, MNRAS, 301, 699
- Marsh T. R. Robinson E. L. & Wood J. H., 1994, MNRAS, 266, 137
- McClintock J. E. Garcia M. R. Caldwell N. & Falco E. E., 2000, IAUC no. 7542
- McClintock J. E. Garcia M. R. Caldwell N. Falco E. E. Garnavich P.M. & Zhao P., 2001, astro-ph/0101421
- Paczyński B., 1970, Acta Astron., 20, 47
- Pan H. C. Skinner G. K. Sunyaev R. A. & Borozin K. N., 1995, MNRAS, 274, L15
- Patterson J., 2000, IAUC no. 7412
- Pols O. R. Tout C. A. Eggleton P. P. & Han Z., 1995, MNRAS, 274, 964
- Portegies Zwart S. Verbunt F. & Ergma E., 1997, A&A, 321, 207
- Pylyser E. & Savonije G., 1988, A&A, 191, 57
- Rhoades C. E. Jr. & Ruffini R., 1974, Phys. Rev. Lett., 32, 324
- Sanchez-Fernandez C. Zurita C. Casares J. Shahbaz T. & Castro-Tirado A., 2000, IAUC no.7506
- Sarna M. J., Dhillon V. S., Marsh T. R. & Marks P. B., 1995, MNRAS, 272, 1336
- Tanaka Y. & Lewin W. H. G., 1995, in: "X-ray Binaries", eds. by W. H. G. Lewin, J. van Paradijs and E. P. J. van den Heuvel, p. 126
- Tanaka Y. & Shibasaki N., 1996, ARA&A, 34, 607
- Tauris Th. M. & Savonije G-J., 1999, A&A, 350, 928
- van den Heuvel E.P.J., 1983, in "Accretion driven stellar X-ray sources" ed. by W.H.G.Lewin&E.P.J.van den Heuvel, p.303
- Verbunt F. & Zwaan C., 1981, A&A, 100, L7
- Webb N. A., Naylor T., Ioannou Z., Charles P. A. & Shahbaz T., 2000, MNRAS, 317, 528
- Wagner R. M. Foltz C. B. Starrfield S. G. & Hewett P., 2000, IAUC no. 7542
- Wagner R. M. Foltz C. B. Shahbaz T. Charles P. A. Starrfield S. G. & Hewett P., 2001, ApJL., in press